PARTON CASCADES, SMALL x, MULTIPLE INTERACTIONS, AND SATURATION*

Gösta Gustafson

Department of Theoretical Physics, Lund University
Sölveg. 14A, 22362 Lund, Sweden
gosta.gustafson@thep.lu.se

(Received October 14, 2011)

In this paper I discuss the dynamics of particle production in high energy reactions. It includes parton cascades and hadronization in e^+e^--annihilation, small x evolution including the Double Leading Log approximation and the BFKL equation, saturation at high densities and the BK equation, and finally the Lund Dipole Cascade model for high energy collisions, which is implemented in the DIPSY MC.

DOI:10.5506/APhysPolB.42.2581
PACS numbers: 12.38.–t, 13.60.Hb, 13.85.–t

1. Introduction

In e^+e^--annihilation the total hadronic cross-section is given by the probability to produce an initial $q\bar{q}$ pair, which is determined by QED. The effects of the strong interaction is here only a correction with relative magnitude α_s/π. The emission of a gluon cascade is, however, essential for the properties of the final state, although it does not change the total cross-section. Here, angular ordering is crucial for the result, and the dipole formulation particularly convenient.

DIS and hadronic collisions are more complicated. In a high energy ep or pp collision the initial partons in a target proton develop virtual parton cascades. A projectile can interact with any of the partons in the cascade, which implies that the total cross-section grows with increasing collision energy. The development of the cascade in this "initial state radiation" determines the inclusive total and elastic cross-sections, but for exclusive final states also "final state radiation" has to be added. In the initial state radiation the virtualities are space-like. The final state radiation is more

* Presented at the LI Cracow School of Theoretical Physics "Soft Side of the LHC", Zakopane, Poland, June 11–19, 2011.

similar to the cascades in e^+e^--annihilation; it does not change the inclusive cross-sections, and the virtualities are time-like. Thus in DIS and hadronic collisions we have two different problems, the total cross-section and the final state properties. There are also two different hard scales, Q^2 and s, while in e^+e^--annihilation there is only one, $Q^2 = s$.

At high energies and small x, gluon cascades and the $1/z$ pole in the splitting function are most important. For large Q^2 this leads to the DLL approximation, and for limited Q^2 to BFKL evolution.

The high density of partons in a proton also implies that at high energies the projectile may interact with more than one parton in the target. As the total interaction probability must not be larger than one, the effective gluon density must "saturate". At high energy the impact parameter is related to the conserved angular momentum, $b \approx L/k$. The interaction probability for fixed b is, therefore, limited by 1, and a description of multiple interactions and saturation is most easy in impact parameter space.

The outline of these notes is first particle production in e^+e^--annihilation with time-like cascades and hadronization in Secs. 2 and 3, followed by small x evolution in Sec. 4 and saturation in Sec. 5, and finally, a discussion of dipole models for high energy pp collisions and DIS in Sec. 6.

2. Time-like cascades

2.1. Bremsstrahlung

In classical electrodynamics the radiation of bremsstrahlung photons is given by the expression (see *e.g.* Ref. [1])

$$dn_\gamma \sim \frac{d^3k}{\omega} \left| \int d^4x\, \boldsymbol{j}(x) \boldsymbol{A}^*(x) \right|^2 . \tag{1}$$

For a charged particle moving along the trajectory $\boldsymbol{x} = \boldsymbol{r}(t)$ we get the current (the charge is denoted g, as the result is the same in QCD)

$$\boldsymbol{j} = g\, \boldsymbol{v}(t)\, \delta(\boldsymbol{x} - \boldsymbol{r}(t)) . \tag{2}$$

With a photon field $\boldsymbol{A} \sim \boldsymbol{\epsilon} e^{-i(\omega t - \boldsymbol{k}\boldsymbol{x})}$ we find, after division and multiplication by $(1 - \boldsymbol{n}\boldsymbol{v})$ and a partial integration, the amplitude

$$\mathcal{M} = \int d^4x\, \boldsymbol{j}(x) \boldsymbol{A}^*(x) = ig \int dt\, \frac{dX}{dt}\, e^{i\omega(t - \boldsymbol{n}\boldsymbol{r}(t))} , \tag{3}$$

where

$$X = \frac{\boldsymbol{\epsilon}\boldsymbol{v}(t)}{\omega(1 - \boldsymbol{n}\boldsymbol{v}(t))} , \qquad \boldsymbol{n} = \frac{\boldsymbol{k}}{\omega} . \tag{4}$$

For soft emissions (small ω) the exponential is approximately constant in regions, where $d\boldsymbol{v}/dt \neq 0$, which implies that

$$\mathcal{M} \;\propto\; (X_f - X_i)\,, \tag{5}$$

$$dn \;\sim\; \alpha\,\frac{d\omega}{\omega}\,d\Omega\left|\frac{\boldsymbol{\epsilon}\boldsymbol{v}_f}{1-\boldsymbol{n}\boldsymbol{v}_f} - \frac{\boldsymbol{\epsilon}\boldsymbol{v}_i}{1-\boldsymbol{n}\boldsymbol{v}_i}\right|^2\,, \tag{6}$$

where $\boldsymbol{v}_i$ and $\boldsymbol{v}_f$ are the velocities before and after the radiation. (For large ω the emission is, however, sensitive to details in the trajectory.)

2.2. Dipole radiation

For emission from pair production of a positive and a negative particle, moving along trajectories $\boldsymbol{r}_+$ and $\boldsymbol{r}_-$, we get the current

$$\begin{cases} t<0: & \boldsymbol{j} = 0\,, \\ t>0: & \boldsymbol{j} = +g\,\boldsymbol{v}_+(t)\,\delta(\boldsymbol{x}-\boldsymbol{r}_+(t)) - g\,\boldsymbol{v}_-(t)\,\delta(\boldsymbol{x}-\boldsymbol{r}_-(t))\,. \end{cases} \tag{7}$$

Thus we see that we get the same result as in Eq. (6), only with the replacements $\boldsymbol{v}_f \to \boldsymbol{v}_+$ and $\boldsymbol{v}_i \to \boldsymbol{v}_-$.

In the c.m.s. system the matrix element for photon emission becomes

$$|\mathcal{M}|^2 \propto \frac{4}{\omega^2\sin^2\theta} = \frac{(p_+p_-)}{(p_+k)(p_-k)}\,. \tag{8}$$

We note that the last expression is relativistically invariant, and thus can be used in any Lorentz frame.

We can compare this result with the expressions from the relevant Feynman diagrams. The two factors in the denominator in Eq. (8) correspond to the propagators $1/(p_+ + k)^2 = 1/[2(p_+k)]$ and $1/(p_- + k)^2 = 1/[2(p_-k)]$ obtained when the photon is emitted from the positive and negative parent respectively. Coherent emission from the two parents give the "dipole formula" in Eq. (8). Denoting the particles with momenta p_+, p_-, and k by the numbers 1, 2, and 3, and defining $s_{ij} = (p_i + p_j)^2$, we also get (including a proper factor $1/\pi$)

$$dn = \frac{\alpha}{\pi}\frac{d\,s_{13}\,d\,s_{23}}{s_{13}\,s_{23}} = \frac{\alpha}{\pi}\frac{d\,k_\perp^2}{k_\perp^2}\,d\,y\,, \tag{9}$$

where

$$k_\perp^2 = \frac{s_{13}\,s_{23}}{s} \qquad \text{and} \qquad y = \tfrac{1}{2}\ln\frac{s_{23}}{s_{13}} \tag{10}$$

represent the transverse momentum and the rapidity in the dipole rest frame. For gluon emission in QCD we get the same expression with the finestructure constant α replaced by $N_c\alpha_s/2$. (For radiation from quarks there is a suppression factor $(1 - 1/N_c^2)$, which is not present for dipoles formed by gluon charges.)

2.3. Angular ordering

With the help of Eq. (8) the dipole emission can also be written

$$d\,n \sim \alpha \frac{d\,\omega}{\omega} d\,\Omega \frac{a_{12}}{a_{13}a_{23}} \qquad \text{with} \qquad a_{ij} \equiv 1 - \boldsymbol{n}_i \boldsymbol{n}_j = 1 - \cos\theta_{ij}\,, \tag{11}$$

where $\boldsymbol{n}_i$ is the direction of particle i, and θ_{ij} is the angle between $\boldsymbol{n}_i$ and $\boldsymbol{n}_j$. As in Eq. (9) particle 3 corresponds to the emitted photon or gluon. The last factor can be rewritten in the form

$$\frac{a_{12}}{a_{13}a_{23}} = \frac{1}{2}\left[\frac{a_{12} - a_{13} + a_{23}}{a_{13}a_{23}} + (1 \leftrightarrow 2)\right] \equiv \frac{1}{2}\left[X_1 + X_2\right]. \tag{12}$$

The first term in the parenthesis (X_1) is non-singular when $a_{23} \to 0$. Averaging this term over the azimuth angle, ϕ, around $\boldsymbol{n}_1$, keeping the polar angle θ_{13} fixed, we get

$$\frac{1}{2\pi}\int X_1 d\phi = \frac{2}{a_{13}}\theta(\theta_{12} - \theta_{13})\,. \tag{13}$$

A similar expression is obtained when averaging X_2 for fixed angle θ_{23}. Thus approximating X_1 and X_2 by these averages, the emission corresponds to *independent emission* from two emitters within the angular ordered regions $\theta_{13} < \theta_{12}$ and $\theta_{23} < \theta_{12}$, respectively.

2.4. More gluons

The emission of *two gluons* is considerably more complicated. In a compressed form the lowest order result for $q\bar{q}gg$ final states takes three full pages in Ref. [2]. However, when the emissions are *strongly ordered*, *i.e.* when $p_4 \ll p_3 \ll W$, where p_3 and p_4 are the gluon momenta, the result factorizes, and thus simplifies considerably. In a semiclassical picture the hardest gluon is emitted first from the $q\bar{q}$ dipole. This gluon carries away colour charge and thus changes the current responsible for subsequent softer emissions. If the first emission produces *e.g.* a red quark, a blue–antired gluon, and an antiblue antiquark, then the red–antired charges radiate coherently as a colour dipole formed by the quark and the gluon. In the rest frame of this dipole the distribution is also given by the expression in Eq. (9). In the same way the blue and antiblue charges radiate coherently as a colour dipole formed by the gluon and the antiquark [3]. (There is also a colour-suppressed term corresponding to a dipole spanned between the quark and the antiquark, with relative weight $-1/N_c^2$.) The emission of a gluon with transverse momentum $k_\perp$ is determined by an average of the current in Eqs. (1), (3) over the "Landau–Pomeranchuk formation time" $\tau \sim 1/k_\perp$. Thus the ordering of the gluons is determined by their transverse momenta, when *measured locally in the emitting dipole rest frame.*

This result can be generalised so that the emission of *many gluons* can be described as a dipole cascade [4]. The phase space for the emissions can be represented by the $(y, \kappa = \ln k_\perp^2)$ diagram shown in Fig. 1. This formulation of the time-like parton cascade is implemented in the ARIADNE MC [5], which very successfully reproduces experimental data from LEP and other e^+e^- colliders.

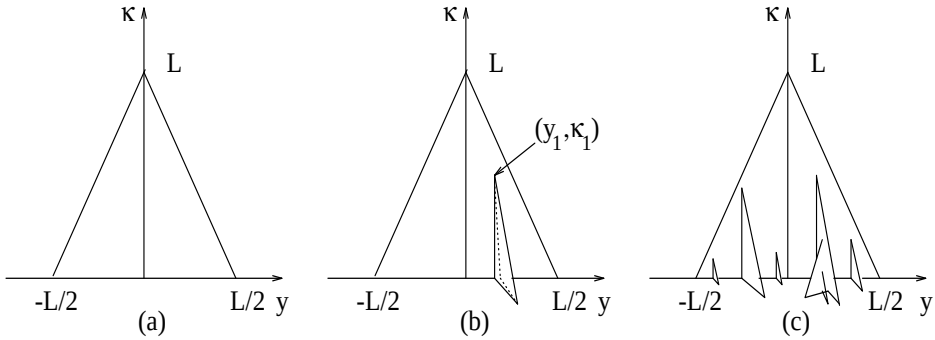

Fig. 1. (a) The phase space for gluon emission in e^+e^--annihilation is a triangular region in the $(y, \kappa \equiv \ln k_\perp^2)$-plane. The height of the triangle is given by $L = \ln s$. (b) When one gluon is emitted at (y_1, κ_1) the phase space for a second (softer) gluon is represented by the area of this folded surface. (c) Each emitted gluon increases the phase space for softer gluons. The total phase space is represented by this multifaceted surface.

The phase space in Fig. 1 apparently has a fractal structure. It is possible to define a fractal dimension given by $D = \sqrt{2N_c\alpha_s/\pi}$ [6]. As $\alpha_s(k_\perp^2)$ is running this is a so-called multifractal. It has been discussed if this feature is responsible for the "intermittency" signal observed in experimental data. However, later it has been realized that a large fraction of the observed effect is related to BE correlations.

3. Hadronization

Quark confinement can be understood if the colour field is compressed to a flux tube by a gluon condensate in vacuum. In an e^+e^--annihilation event a string-like field is stretched out between a quark and an antiquark, and when enough energy is stored in the field, it can break due to the production of a new $q\bar{q}$ pair. A space-time picture of this process is shown in Fig. 2.

In the Lund model the probability for a definite final state is given by the product of a phase space factor and the exponent of a constant times the space-time area spanned by the string before it breaks, denoted by A in Fig. 2 [7]. This expression can be interpreted as a Wilson loop integral, or

an imaginary part of the string action. An important feature of the result is boost invariance, which is also a property of a homogenous longitudinal electric field.

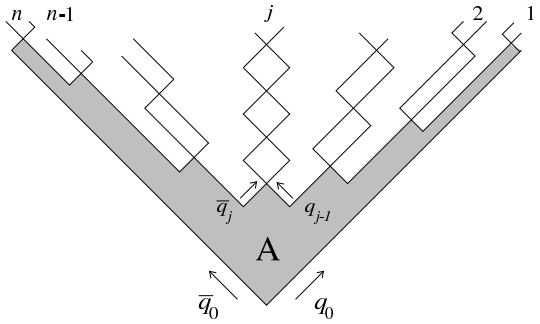

Fig. 2. The hadronization of a high energy $(q_0, \bar{q}_0)$ system in a (x, t) diagram. The hadrons can be ordered in "rank", 1, 2, ... j, ... n. This ordering agrees on average, but not in every case, with the ordering in rapidity.

A gluon carries colour and anticolour charges, and in the Lund string hadronization model it behaves as a transverse excitation on the stringlike field, stretched between a quark and an antiquark [8]. In a three-jet event the string gets a transverse boost, and in the break-up the hadrons are produced around two hyperbolae in momentum space, as shown in Fig. 3 [9]. Thus

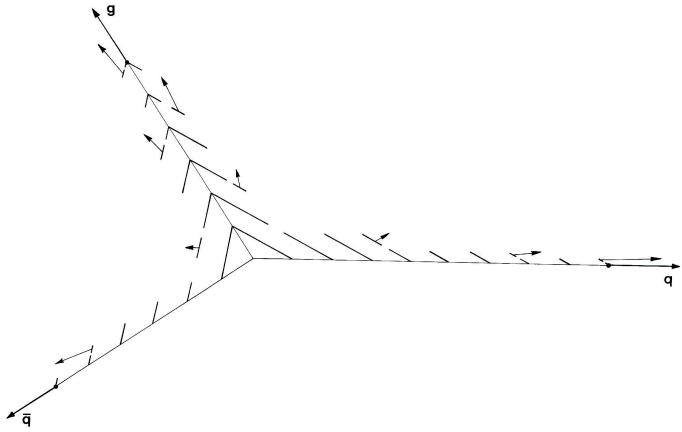

Fig. 3. The space-time development of a quark–antiquark–gluon event. The string is stretched from the quark to the antiquark via the gluon, which moves like a pointlike kink carrying energy and momentum. The string breaks by the production of new $q\bar{q}$ pairs, and the final state contains three jets. Soft particles formed in between the jets get a boost by the transverse motion of the string.

fewer particles are produced in the angular region opposite to the gluon jet, and this asymmetry was experimentally confirmed, first by the JADE detector at the PETRA collider [10].

Gluon radiation is singular for soft and collinear emissions. A very important feature of the string hadronization model is that it is *infrared stable*. The motion of a soft transverse gluon is soon stopped by the tension in the attached strings. In the subsequent string motion the gluon kink is split into two corners, which do not carry energy or momentum and which are connected by a straight string piece, as shown in Fig. 4 (a). The energy in the small sections close to the quark and the antiquark is not sufficient for a hadron, and all breakups will occur in the central string piece, which is stretched and breaks up in the same way as the straight string in Fig. 2. The string motion with a collinear gluon is shown in Fig. 4 (b), and also here the effects of the gluon goes to zero in the collinear limit.

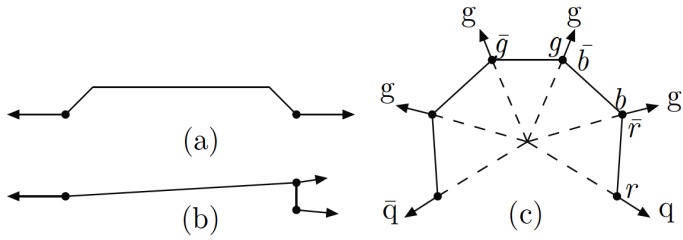

Fig. 4. (a) A soft transverse gluon will soon lose its energy. The kink on the string is split in two corners and a straight string piece is stretched in a way similar to a one-dimensional string. (b) Also for a collinear gluon the energy in the string between the quark and the gluon is too small for a breakup of the string. (c) In a state with many gluons the string is stretched from the quark to the antiquark via the colour-ordered gluons, in the figure from red to antired, from blue to antiblue *etc.*

The situation in Fig. 3 can be directly generalized to many gluons. The string is here stretched from the quark to the antiquark via the colour-ordered gluons, as shown in Fig. 4 (c).

4. Spacelike cascades

As discussed in the introduction, DIS and hadronic collisions are more complicated than e^+e^--annihilation. There are two separate scales, Q^2 and s, and two separate problems: inclusive cross-sections and final state properties. The ladder leading up to the hard interaction (solid lines in Fig. 5) represents the increased parton density in the initial state, and determines the inclusive total and elastic cross-sections. The partons in these cascades have spacelike momenta, and only those branches in the cascade, which interact with the projectile, can come on shell and produce real final

state particles. For exclusive final states also final state radiation has to be added (dashed lines in Fig. 5). This phase is more similar to the cascades in e^+e^--annihilation, with timelike virtualities and conservation of probability.

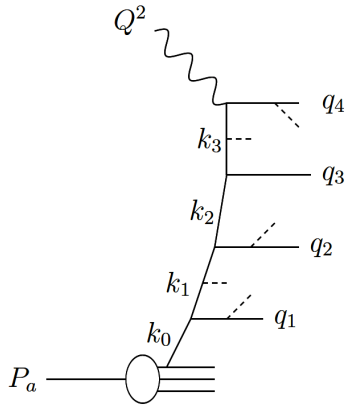

Fig. 5. A DIS event with ISR, solid lines, and FSR, dotted lines. Virtual links are denoted k_i and real emissions q_i.

For high Q^2 and not too small x the ladder is described by ordered DGLAP evolution, where $k_{\perp i} > k_{\perp i-1}$ and the vertices are determined by the quark and gluon splitting functions. For small x gluon ladders are most important, and the evolution dominated by the $1/z$ pole in the gluon splitting function. This pole represents soft emissions, where each step in the ladder corresponds to a large step in rapidity. In this section I will discuss small x evolution in a semiclassical framework, based on Weizsäcker–Williams method of virtual quanta. At high energies more than one parton in the projectile or the target may interact. This problem will be discussed in Sec. 5.

4.1. Weizsäcker–Williams method of virtual quanta

A Coulomb field, which is boosted to high velocity, is contracted to a flat pancake with a dominantly transverse electric field. The pulse will be very short in time, and can be approximated by a δ-function

$$\boldsymbol{E}_\perp \sim g\frac{\boldsymbol{r}}{r^2}\,\delta(t)\,. \tag{14}$$

Here $\boldsymbol{r}$ is the (two-dimensional) distance between the position of the central charge and the point of observation (see Fig. 6). The frequency distribution is given by the Fourier transform, and consequently approximately constant as a function of ω, $E_\perp(\omega) \sim g/r$.

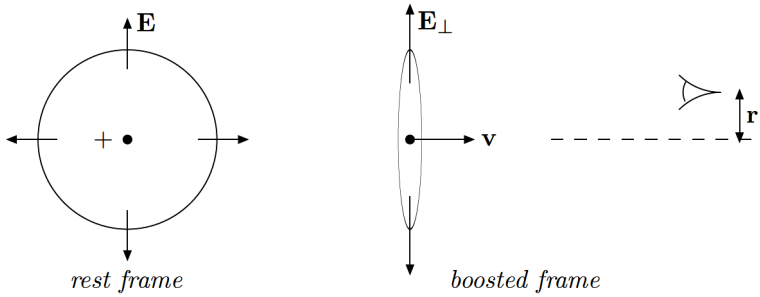

Fig. 6. A Coulomb field in a boosted frame is compressed to a flat pancake.

The electric field is also associated with an orthogonal transverse magnetic field, with the same magnitude. The energy density in the pulse is therefore given by

$$I(\omega) = E_\perp B_\perp \approx E_\perp^2(\omega) \sim g^2 \frac{1}{r^2}\,. \tag{15}$$

The density of photons, or gluons, seen by an observer at point $\boldsymbol{r}$, is obtained by dividing by the energy of a photon, and thus given by

$$dn \sim g^2 \frac{d^2r}{r^2}\frac{d\omega}{\omega} \sim g^2 \frac{d^2q_\perp}{q_\perp^2}\frac{d\omega}{\omega}\,. \tag{16}$$

In the last expression we used that the (two-dimensional) Fourier transform of a wavefunction proportional to $1/r$ is given by $1/q_\perp$.

4.2. Dipoles in space-like cascades

A proton is colour neutral, and the colour field from a parton is always screened by a corresponding anticharge. Let us study the field from a colour dipole formed by a charge at $\boldsymbol{x}$ and an anticharge at $\boldsymbol{y}$ in the transverse plane. The transverse field from these charges in point $\boldsymbol{r}$ is given by (*cf.* Eq. (14) and Fig. 7 (a))

$$\boldsymbol{E} = \boldsymbol{E}_1 + \boldsymbol{E}_2 \propto \frac{\boldsymbol{r}_1}{r_1^2} - \frac{\boldsymbol{r}_2}{r_2^2}\,, \tag{17}$$

where $\boldsymbol{r}_1 = \boldsymbol{r} - \boldsymbol{x}$ and $\boldsymbol{r}_2 = \boldsymbol{r} - \boldsymbol{y}$. Defining $Y = \ln\omega$ and $\boldsymbol{R} = \boldsymbol{r}_1 - \boldsymbol{r}_2$, we find in analogy to Eq. (16) the gluon density in point $\boldsymbol{r}$

$$\frac{d\,n}{d^2r\,dY} \propto \boldsymbol{E}^2 \propto \left(\frac{\boldsymbol{r}_1}{r_1^2} - \frac{\boldsymbol{r}_2}{r_2^2}\right)^2 = \frac{R^2}{r_1^2 \cdot r_2^2}\,. \tag{18}$$

We note that for small r_1 we have $R^2 \approx r_2^2$, and Eq. (18) corresponds to a pure Coulomb field $\propto 1/r_1^2$ from the charge in $\boldsymbol{x}$, while at larger distances, where $R \ll r_1 \approx r_2$, the field is screened and falls off $\sim 1/r^4$.

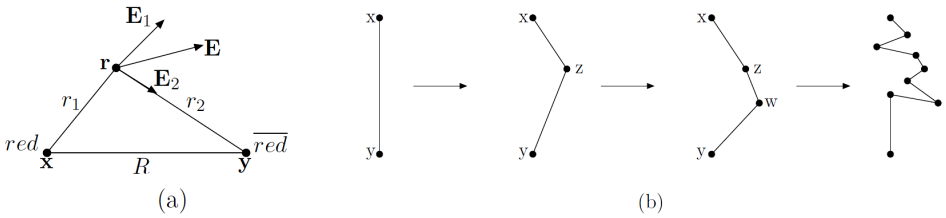

Fig. 7. (a) The transverse colour-electric field in a colour dipole. (b) Gluon emission splits the dipole into two dipoles. Repeated emissions give a cascade, which produces a chain of dipoles.

The essential difference between QCD and QED is that the emitted gluon carries away colour charge. Thus, if *e.g.* the gluon with colour $r\bar{b}$ is emitted from an originally $r\bar{r}$ dipole, the originally red charge is changed to blue, and the dipole is changed to a system of two dipoles, a $b\bar{b}$ dipole formed by the originally red (but now blue) charge and the antiblue charge in the gluon, and a $r\bar{r}$ dipole between the gluon and the original anticharge. In the large N_c limit these dipoles can emit softer gluons independently. The number of dipoles increase as a *cascade* to smaller and smaller rapidities Y, as indicated in Fig. 7 (b).

We note that the density proportional to $d\omega/\omega = dY$ corresponds to the $1/z$ pole in the $q \to qg$ and $g \to gg$ splitting functions, which dominate the parton distribution for very small x.

4.3. Double Leading Log approximation

As mentioned the gluon emission is suppressed when r_1 and r_2 are larger than R, and the distribution in Eq. (18) can be separated in a way very similar to the angular ordering in the time-like cascade. We split the expression in Eq. (18) in the same way as in Eq. (12)

$$\frac{R^2}{r_1^2 \cdot r_2^2} = \frac{1}{2}\left[\frac{R^2 - r_1^2 + r_2^2}{r_1^2\, r_2^2} + (1 \leftrightarrow 2)\right] \equiv \tfrac{1}{2}\left[X_1 + X_2\right] . \tag{19}$$

Here the first term in the parenthesis (X_1) is non-singular when $r_2 \to 0$ (and $r_1^2 \to R^2$). Averaging this term over the azimuth angle, ϕ, around $\boldsymbol{x}$, keeping r_1 fixed, we get

$$\frac{1}{2\pi}\int X_1 d\phi = \frac{2}{r_1^2}\theta(R - r_1) . \tag{20}$$

Thus the gluon emission in Eq. (18) can be approximated by

$$\frac{d\,n}{d^2 r\, dY} \approx \frac{\bar{\alpha}}{2\pi}\left[\frac{d^2 r_1}{r_1^2}\theta(R - r_1) + \frac{d^2 r_2}{r_2^2}\theta(R - r_2)\right] , \tag{21}$$

where we have included the proper numerical factor, and used the notation $\bar{\alpha} = N_c\alpha_s/\pi$. This corresponds to the independent emission from two single charges, confined within the regions $r_i < R$. Thus the dipoles are ordered in size; the daughter dipole is smaller than her parent.

A probe with resolution Q^2 can "see" dipoles in a target with size $r > 1/Q$, while smaller dipoles are not resolved. Although non-ordered dipoles are not totally excluded in the exact expression in Eq. (18), the approximation in Eq. (21) implies that the dipoles in a typical cascade become smaller and smaller. Therefore, for *large* Q^2 ordered emission chains dominate, in which $1/Q < \ldots < r_i < r_{i-1} < \ldots < R$, where R is the size of the initial dipole in the cascade. Calculating the density of dipoles with size r at rapidity y in such a cascade, we get first a contribution from emissions directly from the original dipole

$$\text{direct contribution:} \quad \bar{\alpha}\frac{dr^2}{r^2}dy\,. \tag{22}$$

A two-step contribution is obtained by first emitting a dipole with size r_1 at rapidity y_1, which then emits the observed dipole at a lower rapidity $y < y_1$

$$\text{2 steps:} \quad \bar{\alpha}\frac{dr^2}{r^2}dy\int_r^R \bar{\alpha}\frac{dr_1^2}{r_1^2}\int_y^Y dy_1 = \bar{\alpha}\frac{dr^2}{r^2}dy\left[\bar{\alpha}\ln\left(R^2/r^2\right)(Y-y)\right]\,. \tag{23}$$

Calling the square parenthesis X, we get in three steps

$$\text{3 steps:} \quad \bar{\alpha}\frac{dr^2}{r^2}dy\int_r^R \bar{\alpha}\frac{dr_1^2}{r_1^2}\int_y^Y dy_1\int_r^{r_1} \bar{\alpha}\frac{dr_2^2}{r_2^2}\int_y^{y_1} dy_2 = \bar{\alpha}\frac{dr^2}{r^2}dy\cdot\frac{1}{2^2}X^2\,. \tag{24}$$

Summing contributions from n steps, with $n = 1\ldots\infty$, gives the initial distribution from a single step with the extra factor

$$\sum_n \frac{1}{(n!)^2}X^n = I_0(2\sqrt{X})\,. \tag{25}$$

Here I_0 is a Bessel function, which for large arguments grows like an exponential. With $Y - y = \ln(1/x)$ we therefore get the result

$$\frac{dn}{d^2r\,dY} \sim \exp\left(2\sqrt{\bar{\alpha}\ln\left(R^2/r^2\right)\ln(1/x)}\right)\,. \tag{26}$$

This result represents the *Double Leading Log*, or DLL, approximation, valid for small r (meaning large Q^2) and small x, when both logarithms are large. (We have here assumed a constant coupling $\bar{\alpha}$. For a running coupling $\propto 1/\ln(1/\Lambda^2r^2)$, $\ln(R^2/r^2)$ is replaced by $\ln[\ln(1/\Lambda^2r^2)/\ln(1/\Lambda^2R^2)]$.)

4.4. BFKL evolution

When x is small but Q^2 not large, the integral over the ordered dipoles, r_i, which leads to the factor $(\ln(R^2/r^2))^n/n!$ in Eq. (25), becomes small for large n. Although suppressed, unordered dipole chains become important, in which some r_i may be larger than r_{i-1}. We must then use the full expression for dipole emission in Eqs. (18), (19), instead of the approximation in Eq. (21).

If the rapidity interval $Y-y=\ln(1/x)$ is increased by an amount δY, the density of dipoles $\mathcal{F}(Y,r^2)$ will change in the following way: $\mathcal{F}$ can increase if a dipole with size r' splits forming a dipole r within the interval δY (a gain term), and it can decrease if a dipole of size r splits into two new dipoles (a loss term). This gives the following differential equation

$$\frac{\partial\mathcal{F}\left(Y,r^2\right)}{\partial Y}=\frac{\bar{\alpha}}{2\pi}\left\{\int\frac{d^2r'\cdot r'^2}{r^2(\boldsymbol{r}-\boldsymbol{r}')^2}\mathcal{F}\left(Y,r'^2\right)\cdot 2-\int\frac{d^2r'\cdot r^2}{r'^2(\boldsymbol{r}-\boldsymbol{r}')^2}\mathcal{F}\left(Y,r^2\right)\right\}. \tag{27}$$

(The gain term has a factor 2, because when a dipole splits one or the other daughter can have size r.)

This equation is equivalent to the LL BFKL equation, conventionally formulated in transverse momentum space [11]. An important feature is here that the singularity in the gain term at $\boldsymbol{r}'=\boldsymbol{r}$ is compensated by the singularities in the loss term at $\boldsymbol{r}'=0$ and $\boldsymbol{r}'=\boldsymbol{r}$. To see this more clearly, we note that the integrand in the loss term is symmetric under the exchange $\boldsymbol{r}'\to\boldsymbol{r}-\boldsymbol{r}'$. We can, therefore, make the following replacement

$$\frac{1}{r'^2(\boldsymbol{r}-\boldsymbol{r}')^2}=\left[\frac{1}{r'^2}+\frac{1}{(\boldsymbol{r}-\boldsymbol{r}')^2}\right]\frac{1}{r'^2+(\boldsymbol{r}-\boldsymbol{r}')^2}\to\frac{2}{(\boldsymbol{r}-\boldsymbol{r}')^2[r'^2+(\boldsymbol{r}-\boldsymbol{r}')^2]}. \tag{28}$$

Inserting this expression in Eq. (27) we see that the singularity in the gain and loss terms exactly cancel when $\boldsymbol{r}=\boldsymbol{r}'$. Making also the variable transformation $\boldsymbol{k}=\boldsymbol{r}/r^2$, we arrive at a conventional form for the BFKL equation in momentum space. The cancellation of the singularity at $\boldsymbol{r}'-\boldsymbol{r}=0$ then corresponds to the soft cancellation when $\boldsymbol{k}'_\perp-\boldsymbol{k}_\perp=0$ in momentum space.

To understand the qualitative features of BFKL evolution we approximate the dipole distribution in the gain term by its asymptotic form for small and large r

$$\frac{r'^2}{r^2(\boldsymbol{r}-\boldsymbol{r}')^2}\begin{cases}\approx\frac{1}{r^2} & \text{for } r<r'\\ \approx\frac{r'^2}{r^4} & \text{for } r>r'\end{cases}. \tag{29}$$

This approximation is non-singular when $\boldsymbol{r}' - \boldsymbol{r} \to 0$. In Eq. (27) the singularity in this point was cancelled by the loss term, and in this approximation we, therefore, now only keep the gain term. The result is the equation

$$\frac{\partial \mathcal{F}\left(Y, r^2\right)}{\partial Y} \approx \bar{\alpha} \left\{ \int_{r^2} \frac{dr'^2}{r^2} \mathcal{F}\left(Y, r'^2\right) + \int^{r^2} \frac{dr'^2 r'^2}{r^4} \mathcal{F}\left(Y, r'^2\right) \right\} . \tag{30}$$

We now make the ansatz

$$\mathcal{F}\left(Y, r^2\right) \sim e^{\lambda Y} \left(r^2\right)^{-\gamma-1} \tag{31}$$

which inserted in Eq. (30) gives

$$\lambda \mathcal{F} = \bar{\alpha} \left[\frac{1}{\gamma} + \frac{1}{1-\gamma} \right] \mathcal{F} . \tag{32}$$

This approximation reproduces the qualitative features of the LL BFKL equation, with singularities at $\gamma = 0$ and $\gamma = 1$. The right-hand side has an extreme point for $\gamma = 0.5$, which corresponds to $\lambda = 4\bar{\alpha}$. The approximation somewhat overestimates the contribution from the region $r' \approx r$, and therefore the λ-value is larger than the true value $\lambda = 4 \ln 2\, \bar{\alpha}$. The solution corresponds to an exponential growth for large Y, $\sim e^{\lambda Y} \sim 1/x^{\lambda}$, which is thus faster than the DLL result given by the exponential of the square root of Y.

The BFKL equation describes the density of partons in a cascade, which is relevant for *inclusive* cross-sections. *Exclusive final states* can be calculated in the CCFM model [12, 13], which reproduces BFKL evolution in terms of weights for final states, in which all real gluons are ordered in angle and rapidity. This will be further discussed in Sec. 6.2.

5. Multiple interactions and saturation

5.1. Experimental evidence

The strong increase in the parton density at high energy implies that a single event often contains multiple parton–parton subcollisions. Such events have been observed experimentally [14, 15, 16, 17]. As an example, Fig. 8 shows results from CDF for events with 3 jets + γ, which can only be described including multiple hard subcollisions. *Cf.* also the talk by Rick Field at this school [18].

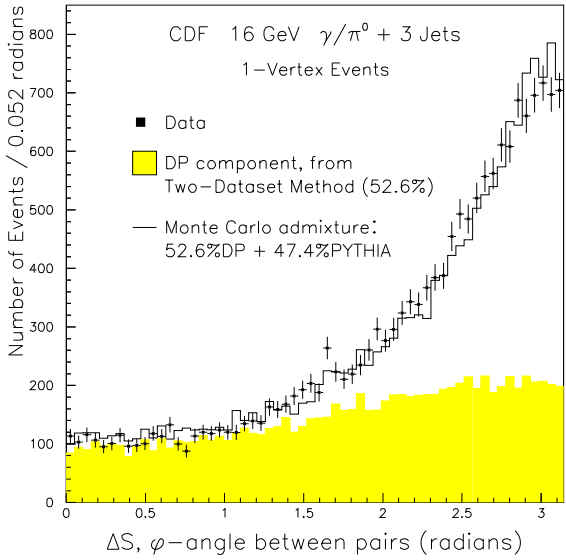

Fig. 8. Reprinted figure with permission from [16]. Distribution in azimuth angle between pairs in events with γ/π^0+ 3 jets from the CDF Collaboration. The shaded (yellow) region shows expectation from double parton scattering.

5.2. Eikonal formalism

As mentioned above, rescattering and multiple interactions are most easily treated in impact parameter space. The result of repeated scattering with momenta $\boldsymbol{k}_{\perp i}$ is given by a convolution in $\boldsymbol{k}_\perp$-space, which corresponds to a multiplication in $\boldsymbol{b}$-space. Thus in impact parameter space the multiple interactions are described by a product of the S-matrix elements for the individual interactions

$$S(b) = S_1(b)S_2(b)S_3(b)\,. \tag{33}$$

If the interaction is driven by absorption into inelastic states i, with weights $2f_i$, the optical theorem gives an elastic amplitude given by

$$T = 1 - e^{-F} \qquad \text{with} \qquad F = \sum f_i\,. \tag{34}$$

For a structureless projectile we then find

$$\begin{cases} d\sigma_{\rm tot}/d^2b = \langle 2T\rangle\,, \\ \sigma_{\rm el}/d^2b = \langle T\rangle^2\,, \\ \sigma_{\rm inel}/d^2b = \left\langle 1 - e^{-\sum 2f_i}\right\rangle = \sigma_{\rm tot} - \sigma_{\rm el}\,. \end{cases} \tag{35}$$

(For the case of a projectile with an internal structure see [19].)

5.3. The BK equation and saturation

Consider scattering of a dipole with charges at transverse coordinates $\boldsymbol{x}$ and $\boldsymbol{y}$ against a dense target at rapidity distance Y. The interaction probability is called $N(\boldsymbol{x}, y, Y)$. Study the change in interaction probability when Y is changed to $Y + \delta Y$. The probability that the dipole has emitted a gluon at point $\boldsymbol{z}$, within the interval δY, is given by Eq. (18). The change in interaction probability is therefore given by [20]

$$\frac{dN(\boldsymbol{x}, y, Y)}{dY} = \frac{\bar{\alpha}}{2\pi} \int d^2z \frac{(\boldsymbol{x} - y)^2}{(\boldsymbol{x} - z)^2(\boldsymbol{z} - y)^2}$$
$$\times [N(\boldsymbol{x}, z, Y) + N(\boldsymbol{z}, y, Y) - N(\boldsymbol{x}, y, Y) - N(\boldsymbol{x}, z, Y)N(\boldsymbol{z}, y, Y)] \ . \quad (36)$$

Here the first two terms in the square bracket give the probability for the new dipoles to interact, the third term is the reduction because the original dipole has disappeared, and the last term avoids double counting by subtracting the probability that both new dipoles interact. This non-linear term prevents the interaction probability to grow beyond 1.

If we now take the average, and furthermore assume that $\langle N \cdot N \rangle = \langle N \rangle^2$ (which may be allowed for a sufficiently dense and homogenous target), we arrive at the Balitsky–Kovchegov equation [20]. It is obvious that this equation has two fixpoints, given by $N = 0$ and $N = 1$. The first corresponds to the weak interaction limit, where the quadratic term can be neglected. The value $N = 1$ corresponds to the black disk limit, where the interaction probability saturates at the unitarity limit.

6. Dipole cascade models for high energy collisions

6.1. Mueller's dipole cascade model

Mueller's model is based on the dipole evolution discussed in Secs. 4.2 and 4.4, which describes LL BFKL evolution in transverse coordinate space [11,21,22]. When a dipole emits a gluon it splits in two dipoles, which in the large N_c limit emit softer gluons independently. The result is a gluon cascade in form of a dipole chain, as illustrated in Fig. 7 (b), where the number of links grows exponentially with rapidity as discussed in Sec. 4.4. Gluon radiation from the colour charge in a parent quark or gluon is screened by the accompanying anticharge in the colour dipole, which suppresses emissions at large transverse separation. Therefore, the dipoles become on average smaller and smaller as the cascade proceeds to smaller rapidities.

When two cascades collide, a pair of dipoles with coordinates $(\boldsymbol{x}_i, \boldsymbol{y}_i)$ and $(\boldsymbol{x}_j, \boldsymbol{y}_j)$ can interact via gluon exchange with the probability $2f_{ij}$, where

$$f_{ij} = f(\boldsymbol{x}_i, \boldsymbol{y}_i | \boldsymbol{x}_j, \boldsymbol{y}_j) = \frac{\alpha_s^2}{8} \left[\log \left(\frac{(\boldsymbol{x}_i - \boldsymbol{y}_j)^2 \boldsymbol{y}_i - \boldsymbol{x}_j)^2}{(\boldsymbol{x}_i - \boldsymbol{x}_j)^2 (\boldsymbol{y}_i - \boldsymbol{y}_j)^2} \right) \right]^2 . \quad (37)$$

We note here in particular that the interaction probability goes to zero for a small dipole. This implies that the singularity in the production probability for small dipoles in Eq. (18) does not give infinite cross-sections. We note also that gluon exchange means exchange of colour between the two cascades. This implies a reconnection of the dipole chains, as shown in Fig. 9, and the formation of dipole chains connecting the projectile and target remnants.

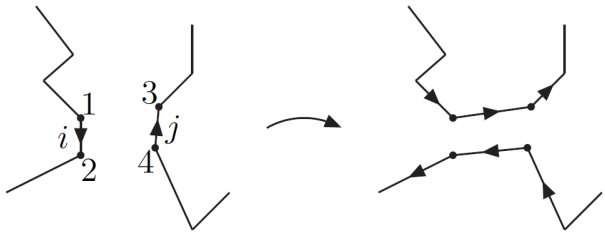

Fig. 9. An interaction between a dipole in the projectile and another in the target due to gluon exchange gives a recoupling of the dipole chains.

In Mueller's model the constraints from unitarity are satisfied using the eikonal formalism. When more than one pair of dipoles interact, colour loops are formed, as shown in Fig. 10. This double interaction is an effect of saturation, corresponding to the non-linear term in the BK equation (36). It is also related to multiple pomeron exchange and pomeron loops in the Regge formalism.

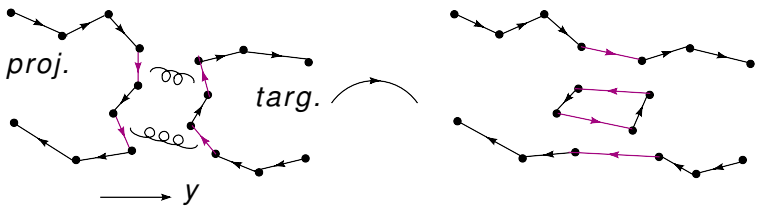

Fig. 10. Double interaction results in a dipole loop, corresponding to a pomeron loop.

In the schematic illustration in Fig. 10, rapidity is growing along the horizontal direction. We here note that if this event was analysed in a Lorentz frame closer to the target, the dipole loop could lie completely within the evolution of the projectile. Thus double interaction in one frame can correspond to a colour loop within the evolution, when viewed in a different Lorentz frame. Such loops are not included in Mueller's model, and are also not taken into account in the BK equation.

6.2. Lund dipole cascade model

The Lund model [23, 24, 25, 26] is a generalisation of Mueller's model, which includes:

— NLL BFKL effects;

— Nonlinear effects in the evolution;

— Confinement effects.

It is implemented in a MC called DIPSY, with applications to collisions between electrons, protons, and nuclei. An incoming virtual photon is here treated as a $q\bar{q}$ pair, with an initial state wavefunction determined by QED. For an incoming proton we make an ansatz in form of an equilateral triangle of dipoles, but after evolution the result is rather insensitive to the exact form of the initial state.

6.2.1. Beyond LL BFKL

The NLL corrections to BFKL evolution have three major sources [27]:

1. *Non-singular terms in the splitting function:* These terms suppress large z-values in the individual parton branchings. Most of this effect is taken care of by including energy-momentum conservation. This is effectively taken into account by associating a dipole with transverse size r with a transverse momentum $k_\perp = 1/r$, and demanding conservation of the lightcone momentum p_+ in every step in the evolution. This gives an effective cutoff for small dipoles.

2. *Projectile-target symmetry:* A parton chain should look the same if generated from the target end as from the projectile end. The corresponding corrections are also called energy scale terms, and are essentially equivalent to the so-called consistency constraint [28]. This effect is taken into account by conservation of the negative lightcone momentum components, p_-.

3. *The running coupling:* This is relatively easily included in a MC simulation process.

6.2.2. Nonlinear effects in the evolution

As mentioned above, multiple interactions produce loops of dipole chains corresponding to pomeron loops. Mueller's model includes all loops cut in the particular Lorentz frame used for the analysis, but not loops contained within the evolution of the individual projectile and target cascades. As for

dipole scattering the probability for such loops is given by α_s, and therefore formally colour suppressed compared to dipole splitting, which is proportional to $\bar{\alpha} = N_c\alpha_s/\pi$. These loops are therefore related to the probability that two dipoles have the same colour. Two dipoles with the same colour form a quadrupole field. Such a field may be better approximated by two dipoles formed by the closest colour–anticolour charges. This corresponds to a recoupling of the colour dipole chains. The process is illustrated in Fig. 11, and we call it a dipole "swing". With a weight for the swing which favours small dipoles, we obtain an almost frame independent result. The number of dipoles in the cascade is not reduced, and the saturation effect is a consequence of the smaller interaction probability for the smaller dipoles. Thus the number of *interacting* dipoles is reduced. Counting only these "effective" dipoles, the swing can be looked upon as a $2 \to 1$, or in some cases $2 \to 0$, transition.

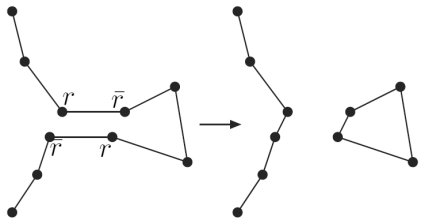

Fig. 11. Two dipoles with the same colour form a colour octet, which may be better approximated by dipoles formed by the closet colour-anticolour pairs. This implies a recoupling of the dipole chains.

6.2.3. Confinement

Confinement is also important. A purely perturbative evolution with massless gluons violates Froissart's bound [29]. This is avoided by giving the gluon an effective mass.

6.3. Results

Here I present some results from the model. For results on diffraction and nucleus collisions, I refer to [19].

6.3.1. Inclusive reactions

The model reproduces successfully the total and elastic cross-sections for *pp* scattering and DIS, as shown in Figs. 12 and 13.

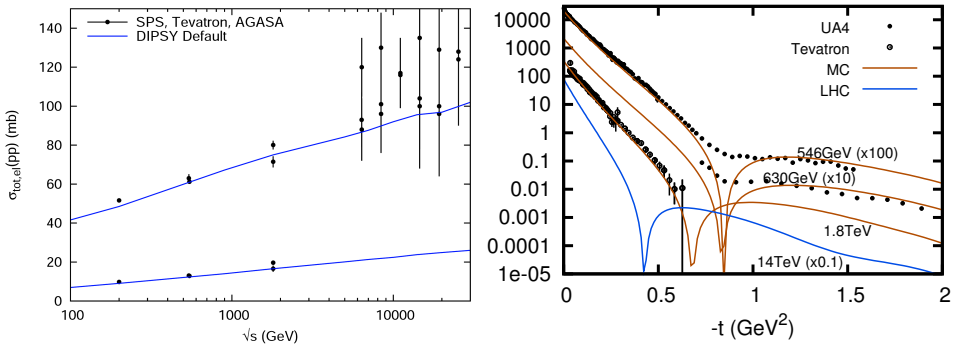

Fig. 12. Total and elastic cross-sections in pp collisions in the dipole cascade model.

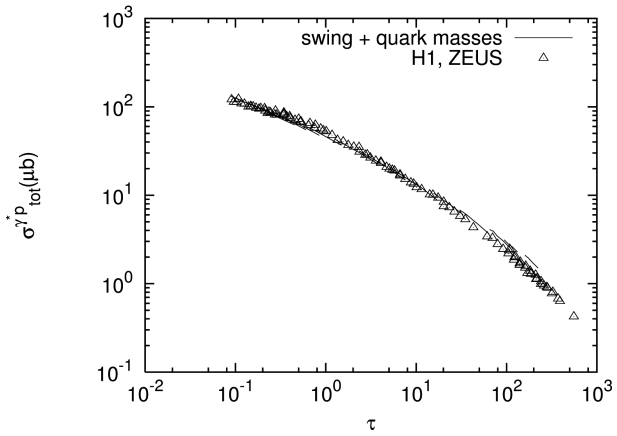

Fig. 13. Total $\gamma^* p$ cross-section presented as a function of the Golec-Biernat–Wüsthoff scaling parameter $\tau = (Q^2/Q_0^2)(x/x_0)^\lambda$, with $Q_0 = 1\text{GeV}$, $x_0 = 3 \times 10^{-4}$, and $\lambda = 0.29$.

6.3.2. Correlations

We define the double parton distribution, and the impact parameter profile F by the relation

$$\Gamma\left(x_1, x_2, b; Q_1^2, Q_2^2\right) \equiv D\left(x_1, Q_1^2\right)\ D\left(x_2, Q_2^2\right)\ F\left(b; x_1, x_2, Q_1^2, Q_2^2\right)\ , \quad (38)$$

where $D(x, Q^2)$ is the single parton distribution. This implies that the cross-section for double hard interactions at midrapidity is given by

$$\sigma^D_{(A,B)} \equiv \frac{1}{(1+\delta_{AB})} \frac{\sigma^S_A \sigma^S_B}{\sigma_{\text{eff}}} \quad (39)$$

with the "effective cross-section", $\sigma_{\rm eff}$, determined by the relation

$$\sigma_{\rm eff} = \left[\int d^2b (F(b))^2\right]^{-1} . \tag{40}$$

F and $\sigma_{\rm eff}$ are often assumed to depend only weakly on x_i and Q_i^2. The MC shows instead that a spike (hotspot) develops for small separations b at larger Q^2, as illustrated in Fig. 14 [30]. This result implies that $\sigma_{\rm eff}$ depends strongly on Q^2 for fixed $\sqrt{s}$, as illustrated in Table I. Part of the correlation is due to fluctuations in the cascade, which can also be taken into account in the MC. Without fluctuations $\int F d^2b$ should be 1. In Table I we see that the fluctuations increase $\int F$ by about 10%, which thus contributes to the correlations given by $\int F^2$.

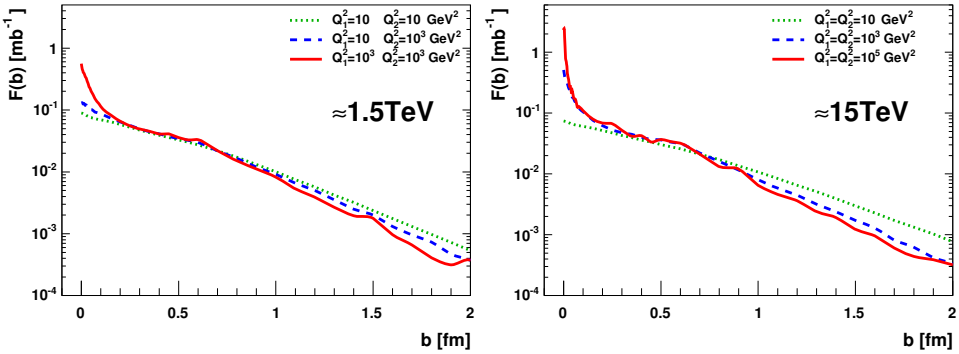

Fig. 14. Correlation function $F(b)$ for midrapidity subcollisions at different Q^2 at Tevatron and LHC energies.

TABLE I

Summary of results for $\sigma_{\rm eff}$ and corresponding integrals of the correlation function F.

Q_1^2	Q_2^2 [GeV^2]	x_1	x_2	$\sigma_{\rm eff}$ [mb]	$\int F$
1.5 TeV, midrapidity					
10	10	0.001	0.001	35.3	1.09
10^3	10^3	0.01	0.01	23.1	1.06
15 TeV, midrapidity					
10	10	0.0001	0.0001	40.4	1.11
10^3	10^3	0.001	0.001	26.3	1.07
10^5	10^5	0.01	0.01	19.6	1.03

6.3.3. Final states

In order to generate exclusive final states, obtained when two dipole cascades collide, we first have to determine which dipoles interact and become recoupled in the way shown in Fig. 9. We note here that BFKL is a stochastic process, and the interactions between different dipole pairs are uncorrelated. This implies that the probability for interaction between dipoles i and j is given by $1 - e^{-2f_{ij}}$, where f_{ij} is determined by Eq. (37).

As mentioned above the BFKL equation describes the density of partons in a cascade, which is relevant for *inclusive* cross-sections. To describe *exclusive final states* it is necessary to take into account colour coherence and angular ordering as well as soft radiation. The latter includes also contributions from the $z = 1$ singularity in the gluon splitting function. These effects are taken into account in the CCFM formalism [12, 13], which also reproduces the BFKL result for the inclusive cross-section.

A very schematic picture of a collision between two dipole cascades is presented in Fig. 15. Here three dipole pairs interact, forming two dipole loops with an additional loop (denoted A) formed within the evolution of the left cascade. Non-interacting branches, like B and C, have to be regarded as virtual and must be reabsorbed.

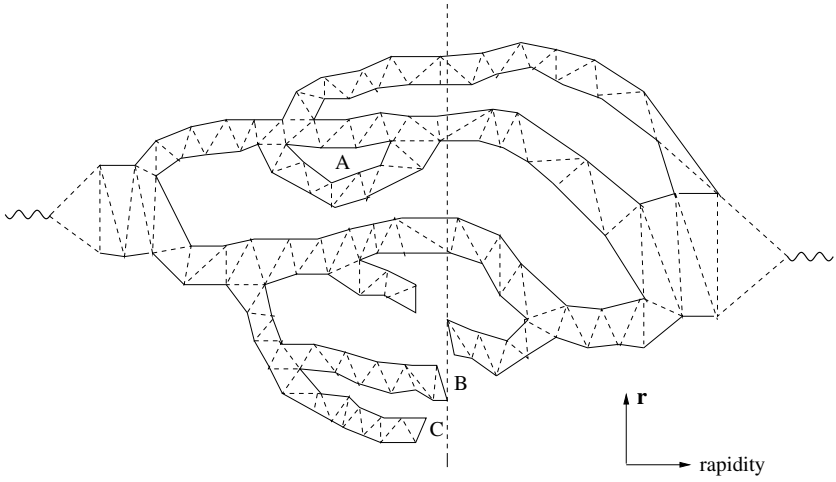

Fig. 15. Schematic picture of a collision between two dipole cascades. A dipole loop within the evolution is denoted A. Non-interacting branches, like B and C have to be regarded as virtual and reabsorbed.

A reformulation of the CCFM model, called the Linked Dipole Chain model, was presented in Ref. [31]. Here it was demonstrated that the inclusive cross-section is fully determined by a subset of the gluons in the CCFM approach, denoted "$k_\perp$-changing" gluons. In Fig. 16 (a), we denote the real

emitted gluons in a ladder $q_{\perp i}$, and the virtual links $k_{\perp i}$. The $k_\perp$-changing emissions $k_{\perp i}$ are either much larger or much smaller than $k_{\perp i-1}$. This also means that $q_{\perp i} \approx \max(k_{\perp i}, k_{\perp i-1})$.

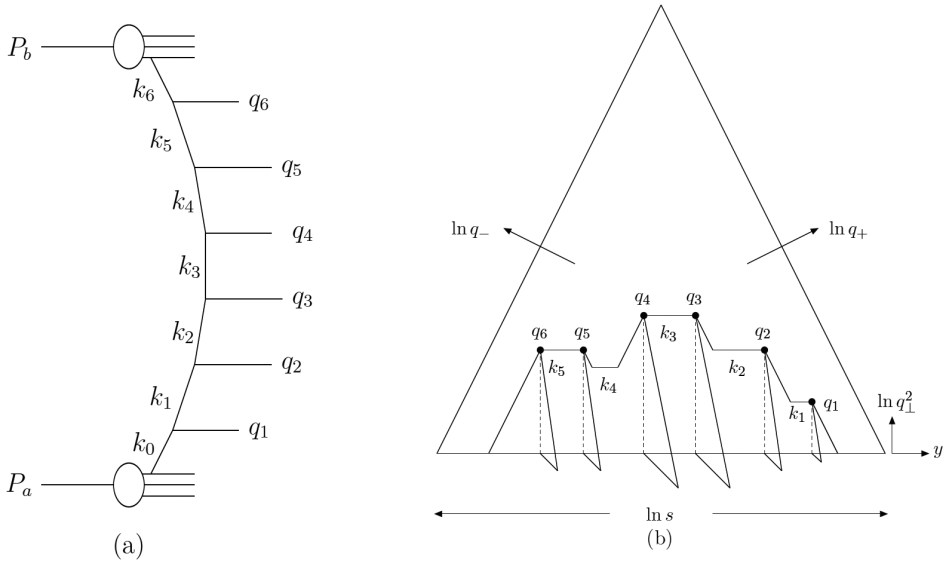

Fig. 16. (a) A parton–parton scattering chain. Virtual links are denoted k_i and real emissions q_i. In BFKL dynamics the transverse momenta are not ordered, and the result should be the same in any Lorentz frame. (b) The same chain in a $(y, \ln q_\perp^2)$ plot. Final state radiation is allowed below the horizontal lines, and on the folds representing transverse jets.

The chain in Fig. 16 (a) is shown in the triangular phase space diagram in Fig. 16 (b). The real gluons q_i are ordered in p_+ and in p_-, and thus also in rapidity or angle. It was also demonstrated that to get the full final states softer emissions have to be added below the horizontal lines in Fig. 16 (b), as final state radiation. This also includes the folds sticking out of the plane, which represent the transverse jets formed by the gluons q_i.

Thus in order to generate exclusive final states we should go through the following steps:

1. Generate cascades for projectile and target;
2. Determine which dipoles interact;
3. Absorb non-interacting chains;
4. Determine final state radiation;
5. Hadronize.

The main problems in this process are due to the large number of small dipoles in the cascades. These have low cross-sections, and are therefore not a big problem for inclusive cross-sections. Because small dipoles correspond to high transverse momenta, they do, however, have a large effect on the properties of the final states. This implies that the result is sensitive to details in the treatment of non-interacting dipoles. Our aim here is therefore not to give very precise predictions, but rather to get insight into the dynamical features of small x evolution and saturation.

As a few examples Figs. 17 and 18 show comparisons with ATLAS data for minimum bias and underlying events at 0.9 and 7 TeV. Fig. 17 shows the η-distribution of charged particles in minimum bias events. The solid line shows the result from the DIPSY MC, and the dotted line the result from PYTHIA. We note that the particle density is well reproduced at 0.9 TeV, but does not grow fast enough with energy, which is a problem also for other MCs which are not tuned individually for each energy. The properties of the underlying event is shown in Fig. 18, which presents the charged multiplicity in the "transverse region", as defined by Rick Field, as a function of the $p_\perp$ of a leading charged particle. The model reproduces quite well the increased density for higher $p_\perp$. More comparisons are found in Ref. [26].

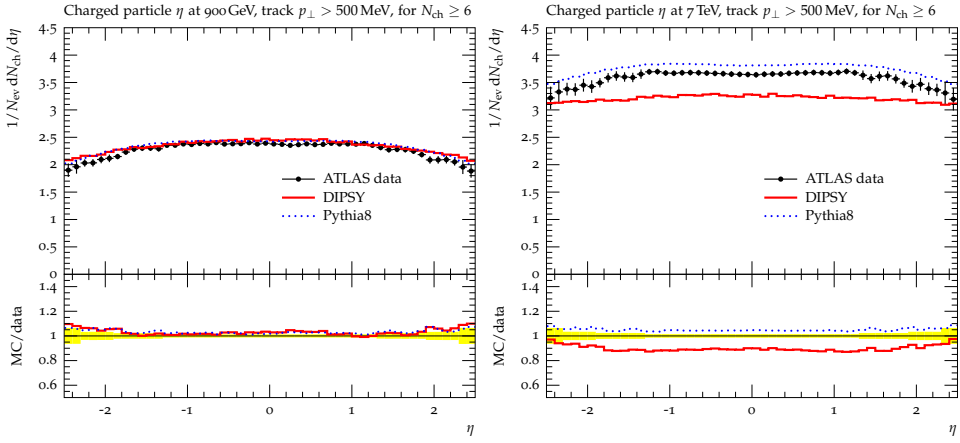

Fig. 17. η-distribution of charged particles at 0.9 and 7 TeV. The solid line shows the result from the DIPSY MC, and the dotted line PYTHIA. Data from the Atlas Collaboration [32].

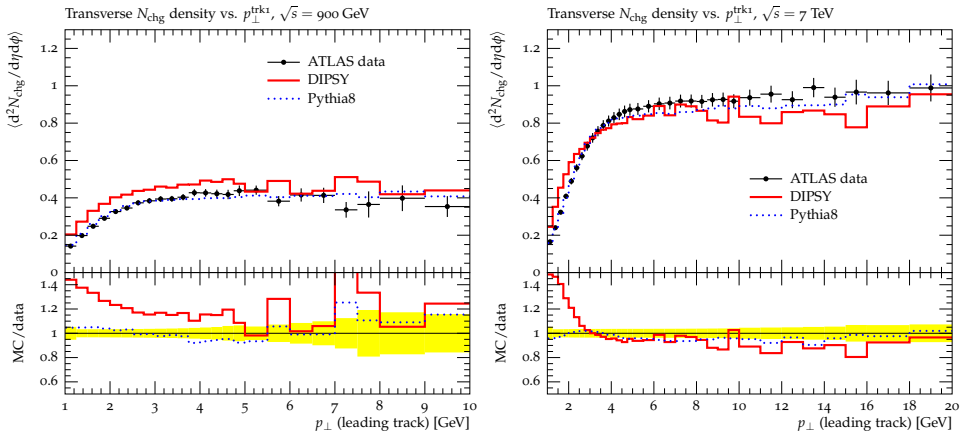

Fig. 18. N_{ch} in transverse region *vs.* $p_\perp$ of leading charged particle. Notation as in Fig. 17. Data from the Atlas Collaboration [33].

6.3.4. Diffractive excitation and nucleus collisions

The model can also be applied to diffractive excitation and to reactions involving nuclei. These phenomena are discussed in [19].

7. Summary

In this paper I have discussed initial and final state radiation in high energy collisions, including small x evolution and saturation. I have also presented the Lund Dipole Cascade model, which is a partonic model for interactions at high energy and density including:

— important non-leading effects in BFKL,

— saturation within the evolution,

— confinement,

— A MC implementation DIPSY.

It gives a good description of inclusive pp and ep cross-sections (including diffraction), and a fair description of exclusive final states (min. bias and underlying event). The model can also be applied to reactions with nuclei, with some early results available. The model contains less input and fewer tunable parameters than other MCs, as the structure functions are determined by BFKL evolution and not fitted to data, and effects of saturation are obtained dynamically, in contrast to a conventional adjustable cutoff for small $p_\perp$ in the hard subcollisions. Our aim is therefore not to give very

precise predictions, but rather to get insight into the dynamical features of small x evolution and saturation in a formalism, which includes correlations, fluctuations, and finite size effects in a way, which to our knowledge is not possible in other approaches.

REFERENCES

[1] J.K. Jackson, *Classical Electrodynamics*, John Wiley and Sons, 1998.

[2] R.K. Ellis, D.A. Ross, A.E. Terrano, *Nucl. Phys.* **B178**, 421 (1981).

[3] Y.I. Azimov, Y.L. Dokshitzer, V.A. Khoze, S.I. Troian, *Phys. Lett.* **B165**, 147 (1985).

[4] G. Gustafson, U. Pettersson, *Nucl. Phys.* **B306**, 746 (1988).

[5] L. Lonnblad, *Comput. Phys. Commun.* **71**, 15 (1992).

[6] G. Gustafson, A. Nilsson, *Nucl. Phys.* **B355**, 106 (1991).

[7] B. Andersson, G. Gustafson, B. Soderberg, *Z. Phys.* **C20**, 317 (1983).

[8] B. Andersson, G. Gustafson, *Z. Phys.* **C3**, 223 (1980).

[9] B. Andersson, G. Gustafson, T. Sjostrand, *Phys. Lett.* **B94**, 211 (1980).

[10] JADE Collaboration., *Phys. Lett.* **B157**, 340 (1985); *Z. Phys.* **C39**, 1 (1988).

[11] A.H. Mueller, *Nucl. Phys.* **B415**, 373 (1994).

[12] S. Catani, F. Fiorani, G. Marchesini, *Nucl. Phys.* **B336**, 18 (1990).

[13] M. Ciafaloni, *Nucl. Phys.* **B296**, 49 (1988).

[14] T. Akesson *et al.* [Axial Field Spectrometer Collaboration], *Z. Phys.* **C34**, 163 (1987).

[15] F. Abe *et al.* [CDF Collaboration], *Phys. Rev.* **D47**, 4857 (1993).

[16] F. Abe *et al.* [CDF Collaboration], *Phys. Rev.* **D56**, 3811 (1997).

[17] V.M. Abazov *et al.* [D0 Collaboration], *Phys. Rev.* **D67**, 052001 (2003) [arXiv:hep-ex/0207046].

[18] R. Field, *Acta Phys. Pol. B* **42**, 2631 (2011), this issue.

[19] G. Gustafson, *Acta Phys. Pol. B* **42**, 2571 (2011), this issue.

[20] Y.V. Kovchegov, *Phys. Rev.* **D61**, 074018 (2000) [arXiv:hep-ph/9905214].

[21] A.H. Mueller, B. Patel, *Nucl. Phys.* **B425**, 471 (1994) [arXiv:hep-ph/9403256].

[22] A.H. Mueller, *Nucl. Phys.* **B437**, 107 (1995) [arXiv:hep-ph/9408245].

[23] E. Avsar, G. Gustafson, L. Lonnblad, *J. High Energy Phys.* **0507**, 062 (2005) [arXiv:hep-ph/0503181].

[24] E. Avsar, G. Gustafson, L. Lönnblad, *J. High Energy Phys.* **01**, 012 (2007) [arXiv:hep-ph/0610157].

[25] C. Flensburg, G. Gustafson, L. Lonnblad, *Eur. Phys. J.* **C60**, 233 (2009) [arXiv:0807.0325 [hep-ph]].

[26] C. Flensburg, G. Gustafson, L. Lönnblad, arXiv:1103.4321 [hep-ph].

[27] G.P. Salam, *Acta Phys. Pol. B* **30**, 3679 (1999) [arXiv:hep-ph/9910492v1].

[28] J. Kwiecinski, A.D. Martin, P.J. Sutton, *Z. Phys.* **C71**, 585 (1996) [arXiv:hep-ph/9602320].

[29] E. Avsar, *J. High Energy Phys.* **0804**, 033 (2008) [arXiv:0803.0446 [hep-ph]].

[30] C. Flensburg, G. Gustafson, L. Lonnblad, A. Ster, *J. High Energy Phys.* **1106**, 066 (2011) [arXiv:1103.4320 [hep-ph]].

[31] B. Andersson, G. Gustafson, J. Samuelsson, *Nucl. Phys.* **B467**, 443 (1996).

[32] G. Aad *et al.* [ATLAS Collaboration], *New J. Phys.* **13**, 053033 (2011) [arXiv:1012.5104 [hep-ex]].

[33] G. Aad *et al.* [ATLAS Collaboration], *Phys. Rev.* **D83**, 112001 (2011) [arXiv:1012.0791 [hep-ex]].